Analysis of multiple time scales in a transistor amplifier

Douglas N. Armstead* and Thomas L. Carroll
US Naval Research Laboratory, Washington, DC 20375

(Dated: May 25, 2004)

A simple class C transistor amplifier is usually considered to be a linear electronic system. It was shown previously in an experiment that when high frequency signals (on the order of $1MHz$) were injected into this low frequency amplifier, the non-linearities of the pn junctions caused period doubling, chaos, and very low frequency oscillations (on the order of $1Hz$). In this paper we present theory and simulations to explain the existence of the low frequency oscillations.

I. INTRODUCTION

In previous work [1] experiments showed that driving a simple one transistor audio amplifier, Fig. 1, with a high frequency (approximately $1MHz$) signal could induce chaos, period doubling, and low frequency (on the order of $1Hz$) switching.

Chaos and period doubling in such a system might be expected based on studies of the diode resonator [2–10], in which a periodic signal is applied to a circuit consisting of an inductor, a resistor, and a diode. The inductor combined with the nonlinear capacitance of the diode form a non-linear resonant system, which may exhibit period doubling or chaos.

In our previous experimental work, we were interested in what sort of non-linear effects might be seen if a low frequency system containing pn junctions (such as our amplifier) was subjected to high frequency rf signals. The rf signals might be accidently produced by nearby communications systems, or they might be intentionally beamed at the circuit in an attempt to disrupt the functioning of the circuit. The inductances of the wires of the circuit combined with the capacitance of the pn junctions in the transistor formed the non-linear resonant system, with a resonant frequency on the order of GHz.

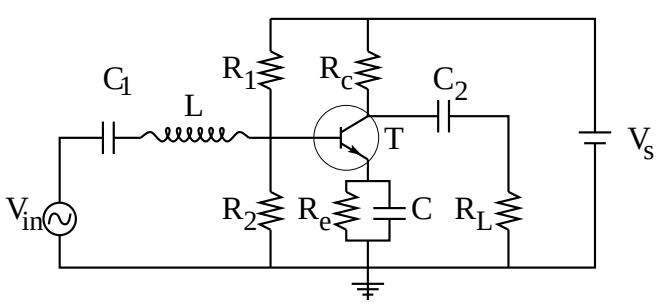

FIG. 1: A simple, stable, audio frequency transistor amplifier. $V_s = 15V$, $R_1 = 40.42k\Omega$, $R_2 = 204.545k\Omega$, $R_c = 15k\Omega$, $R_e = 3.75k\Omega$, $R_L = 1M\Omega$, $C_1 = C_2 = 25\mu F$, $C = 330\mu F$, $L = 2200\mu H$, and the transistor T is of type 2n929. The output of the circuit is across the load resistor, R_L.

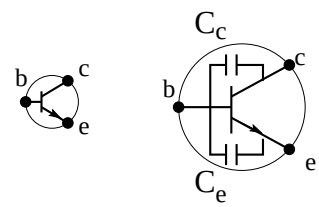

FIG. 2: The transistor has small variable internal capacitances C_c and C_e that are known to be frequency dependent.

The actual rf signals might have frequencies on the order of $1GHz$, but systems that can digitize signals fast enough to study GHz phenomena are still quite expensive, so we added an inductor to the input of the transistor amplifier in order to lower the resonant frequency of the inductor-pn junction combination.

II. EXPERIMENTAL DESCRIPTION

We consider a simple audio frequency transistor amplifier, Fig. 1. The transistor is a $2n929$ bipolar transistor The transistor has variable internal capacitance (Fig. 2) from a number of mechanisms (i.e., junction capacitance, diffusion capacitance) with a magnitude of order $C_o \approx 10^{-11}F$.

This capacitance gives the circuit a natural resonance near the frequency $f_o = 1/\sqrt{4\pi^2 LC_o} \approx 1MHz$ (n.b. The inductor L was explicitly added to make the experiment easier to perform. There are inductances inherent in the wires and typical values give resonances on the order of GHz, which makes data collection difficult.). Driving the circuit with a signal with frequency f near f_o causes the circuit to respond at the driving frequency f and also exhibits a low frequency switching on the order of 5 to $10Hz$. The experimentally determined switching frequency for a range of driving frequencies and driving amplitudes appear in Fig 11.

*Electronic address: armstead@anvil.nrl.navy.mil

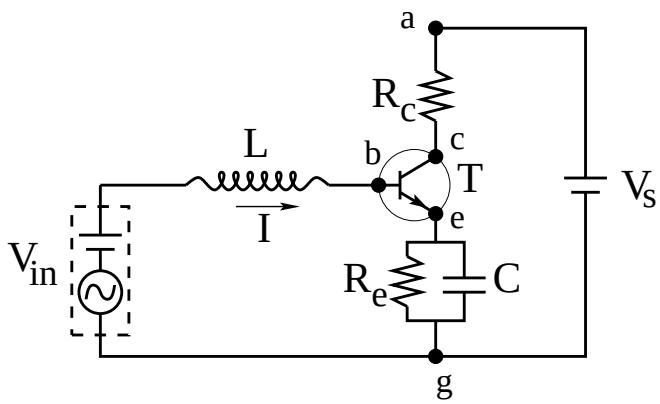

FIG. 3: A much simpler circuit that exhibits the same behavior as Fig. 1. For the numerical work done on this circuit we use the parameters $V_s = 15V$, $R_c = 5k\Omega$, $R_e = 10k\Omega$, $C_o = 20\mu F$, $C = 3\mu F$, $L = 2000\mu H$, $V_{in} = V_{ino} + V_A \sin(2\pi f t)$, $V_{ino} = 2V$.

III. THEORY

In order to simplify our analysis, we eliminate circuit elements which are not necessary for low frequency switching. Experiments and numerical simulations show that C_1 and C_2 are not necessary.

Removing capacitors C_1 and C_2 reduces the dimensionality of the system without substantially changing the dynamics of the circuit. This somewhat simpler circuit (Fig. 3) exhibits similar behavior to the experimental circuit. At the audio frequencies the circuit is designed for, the inductor and the capacitances in the transistor are unimportant. At these low frequencies when the voltage across the base-emitter junction, V_{be}, is below a threshold value, V_o, the transistor is non-conducting. Note that in general we define V_{ab} to be the voltage drop from point a to point b. For the transistor control voltage, V_{be}, above the threshold a small current will flow (at least for a bipolar junction transistor) from the base of the transistor (point b) to the emitter of the transistor (point e). This small current from b to e stimulates a much larger current from the collector (point c) out the emitter. The much larger collector-emitter current is proportional to $V_{be} - V_o$, at least for $V_{be} - V_o$ small. In this mode of operation the transistor acts as a voltage valve. For $V_{be} - V_o \approx 0$ very little current flows and most of the voltage drop across the amplification power source, V_s, occurs across the the collector-base junction (i.e., $V_{ac} \approx 0$ and $V_{cb} \approx V_s - V_{ino}$ where V_s is the amplifier power supply voltage and V_{ino} is the input signal biasing) whereas for large values of $V_{be} - V_o$ a large current flows and most of the current drop is across the resistor R_c (i.e., $V_{ac} \approx V_s - V_{ino}$ and $V_{cb} \approx 0$).

At the frequencies we consider in this paper all four reactive elements in the circuit in Fig. 3 are important: the inductor L, the capacitor C, and the two internal capacitances of the transistor C_c and C_e. As a result, the circuit can be described using four ODEs:

$$\begin{aligned}
\frac{dI}{dt} &= \frac{1}{L}(V_{in} - V_{be} - V_{eg}) \\
\frac{dV_{cb}}{dt} &= \frac{1}{C_c}(V_{ac}/R_c - I_c) \\
\frac{dV_{be}}{dt} &= \frac{1}{C_e}(V_{ac}/R_c + I - I_e) \\
\frac{dV_{eg}}{dt} &= \frac{1}{C}(V_{ac}/R_c - I - V_{eg}/R_e)
\end{aligned} \tag{1}$$

where $V_{in} = V_{ino} + V_A \sin(2\pi f t)$, I is the current through the inductor, and I_c and I_e are the non-linear currents which come from an Ebers-Moll description of the transistor.

$$I_c = I_o[-(e^{-qV_{cb}/kT} - 1) + \alpha(e^{qV_{be}/kT} - 1)$$

$$I_e = I_o[(e^{qV_{be}/kT} - 1) - \alpha(e^{-qV_{cb}/kT} - 1)$$

where $I_o = 10^{-11}$, k is Boltzmann's constant, T is the temperature in Kelvin, and $\alpha = 0.995$ is the fraction of current lost through the base of the transistor.

We now make a number of simplifying assumptions:

- The experimental effect was seen with different types of transistors, including both bipolar and FETs. From this we infer that the details of the nonlinearity of the current function are unimportant, so we approximate the exponential nonlinearity in the current function with a piece-wise linear form (as was done for the diode resonator in [7] and [8]) linearized about the voltage, V_o, at which the non-linearity becomes important.

- Simulations show that the nonlinear capacitance is not necessary for the low frequency oscillations, therefore the type of transistor capacitance is not important, only the fact that it is present, and its approximate value, C_o.

- The collector-base junction is never driven into a forward bias so the V_{cb} contributions to the nonlinear currents are not important. The circuit will not be driven in such a way that the base-emitter junction will receive a large reverse bias.

- The leakage of base current, while important for the proper functioning of a bipolar transistor, is not important for the FETs. In light of this we use $\alpha = 1$.

- The large capacitance of C compared to both the transistor's internal capacitance (i.e., $Co/C \ll 1$) and the inductance L (i.e., $L/(R_E C) \ll 1$) means that the dynamics of V_{eg} are much slower than those of the other variables. As a result, V_{eg} can be treated as a constant compared to the other variables, i.e.,

$$\frac{dV_{ac}}{dt} = \frac{d(V_s - V_{cb} - V_{be} - V_{eg})}{dt} \approx -\frac{dV_{cb}}{dt} - \frac{V_{be}}{dt}. \quad (2)$$

With these assumptions we rewrite the physical representation of the circuit Eqs. (1) in more natural coordinates:

$$\begin{aligned} \frac{dx_1}{d\phi} &= \gamma[\sin(2\pi\phi) - x_3 - y] \\ \frac{dx_2}{d\phi} &= -\delta[x_1 + 2x_2 - 2\kappa x_3 H(x_3)] \\ \frac{dx_3}{d\phi} &= \delta[x_1 + x_2 - \kappa x_3 H(x_3)] \\ \frac{dy}{d\phi} &= \epsilon[\lambda(x_1 + x_2) - y - y_o] \end{aligned} \quad (3)$$

where $x_1 = R_c I/V_A$, $x_2 = V_{ac}/V_A$, $x_3 = (V_{be} - V_o)/V_A$, $y = V_{eg}/V_A - y_o$, $y_o = (V_{ino} - V_o)/V_A$, $\phi = ft$, $\gamma = \frac{R_c}{fL}$, f is the frequency of the input signal, $\delta = \frac{1}{fR_cC_o}$, $\epsilon = \frac{1}{fR_eC}$, $\lambda = Re/Rc$, $\kappa = \frac{qR_cI_o}{kT}\exp(qV_o/kT)$, and $H(x)$ is the Heavyside step function, which has a value of 0 for $x < 0$ and 1 for $x > 0$. For the relevant circuit parameters (see Fig. 3) all parameters that appear in Eqs. (3) are of order 1, except $\epsilon \sim O(10^{-3})$ and $\kappa \sim O(10^3)$.

Numerical integration of Eqs. (3) yields behavior that is substantially the same as is seen in the experiment. The variables x_1, x_2, and x_3 are typically periodic in the drive frequency (i.e., have a period of one in the ϕ time parameterization) and are bi-stable. Figure 4(a) shows x_1, x_2, and x_3 in their high amplitude waveforms and Fig. 4(b) shows x_1, x_2, and x_3 in their low amplitude wave forms. These two sets of stable periodic waveforms that x_1, x_2, and x_3 execute are for the same value of y, in this case $y = 1.15$. The waveforms gradually evolve as y slowly changes until the system switches from one waveform set to the other.

This switching behavior is captured in Fig. 5 which shows x_2, the normalized voltage across the resistor R_c, against y strobed once per drive cycle. Figure 5 shows the low frequency switching between the high amplitude state and the low amplitude state. In the high amplitude state (shown with large pluses) a large rectified current flows through R_c and into the transistor collector. This DC biased current flows through the transistor and charges capacitor C, increasing y until $y = y_{max}$ when the system switches into the low amplitude state (shown with small crosses). In the low amplitude state for $y_{max} > y > y_*$, x_3 is strictly less than zero. As a result the transistor does not conduct and there is no longer a rectified current flowing through R_c. Even after x_3 starts making excursions above $x_3 = 0$, as in the example shown in Fig. 4, the rectified current is much smaller than in the high amplitude state. With rectification effectively stopped throughout the low amplitude state, time average of x_1 and x_2 over one drive oscillation (DC level) approaches zero. As a result, charging stops and the capacitor C discharges through R_e, the resistor in parallel with C, so y drops. As y nears y_{min}, the lower end of its range, the system becomes unstable, causing the system to switch back into the high amplitude state. This instability causes the system to switch back into the high amplitude state in a number of ways, depending on the input signal frequency. The system may switch directly from the period one low amplitude state to the high amplitude state, it may first pass into a period doubling cascade and become chaotic before switching to the high amplitude state, or the system may even pass through a period doubling cascade and then through an inverse period doubling cascade before switching to the high amplitude state.

The low frequency switching is part of a hierarchy of time scales relevant to this system. At the fastest time scales (times of order $1/\kappa \ll 1$) there is the reaction of the system to the transistor turn on, (i.e., the non-linear currents I_c and I_e switch on.) There is an intermediate time scale (times of order 1) associated with the driving frequency. At the slowest time scales (times of order $1/\epsilon \gg 1$) is the variation in the slow variable y, which is responsible for the slow switching observed in this system.

IV. SINGULAR PERTURBATION THEORY

This hierarchy of time scales makes singular perturbation theory (SPT) [11] an attractive approach. In SPT one makes use of a small parameter to treat the fast and slow evolution of a system separately. One does this by using two different parameterizations of time, t and $\tau = \epsilon t$. Consider an example of the van der Pol oscillator [11] in the t parameterization

$$\begin{aligned} \frac{dx}{dt} &= x - x^3/3 - y \\ \frac{dy}{dt} &= \epsilon x \end{aligned} \quad (4)$$

or equivalently in the τ parameterization

$$\begin{aligned} \frac{dx}{d\tau} &= \frac{1}{\epsilon}(x - x^3/3 - y) \\ \frac{dy}{d\tau} &= x \end{aligned} \quad (5)$$

where $\epsilon \ll 1$. The van der Pol oscillator, Eq. (4) is a relaxation oscillator. Its cycle consists of four pieces: a slow evolution of x and y, a rapid, nearly discontinuous jump in x while y stays roughly constant, another slow evolution of x and y, and one final rapid jump in x with y roughly constant. These four pieces of the cycle can be neatly split from each other and, in the limit $\epsilon \to 0$ are described by two sets of equations. The fast evolving pieces are governed by a "fast" set of equations (from the t parameterization of time) and the slowly evolving

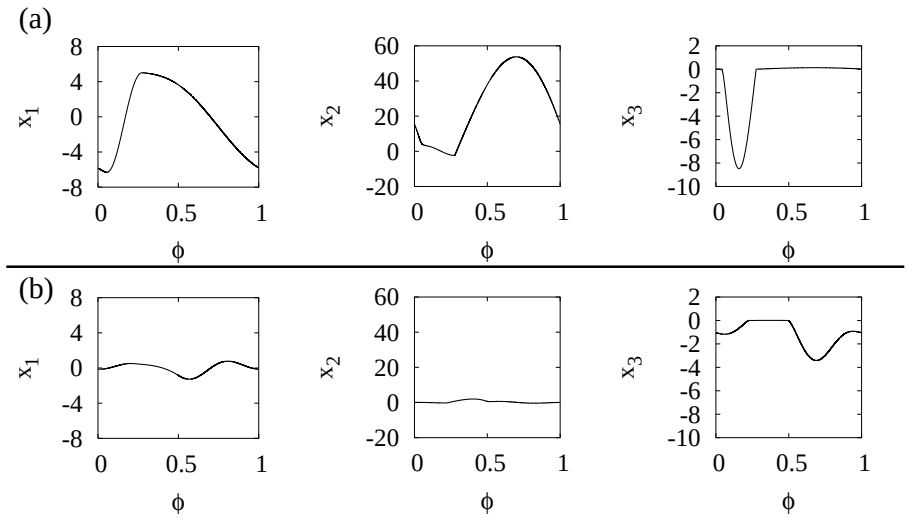

FIG. 4: Numerical integration of Eq. (3) over one period of the drive function. Set (a) is from the high amplitude state and shows the high amplitude wave forms of x_1, x_2, and x_3. Set (b) is from the low amplitude state and shows the low amplitude wave forms of x_1, x_2, and x_3. Both sets are for the same value of $y = 1.15$.

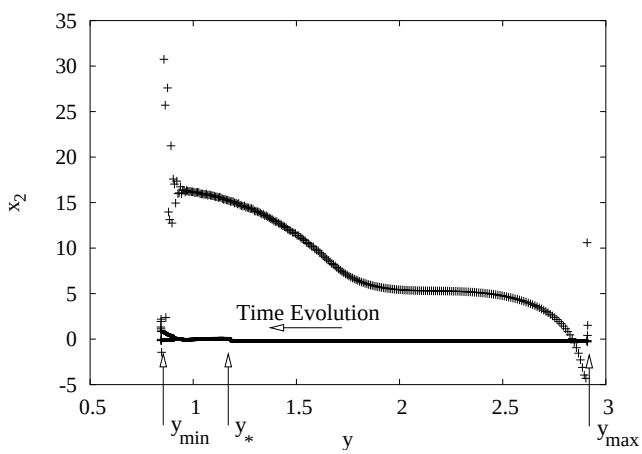

FIG. 5: Numerical integration of Eq. (3) over one slow switching cycle strobed once per drive cycle. The system evolves along the orbit in a clockwise sense. Initially in the low amplitude state, shown with small ×s, the system switches to the high amplitude state, shown with large +s, at $y = y_{min}$ and switches from the high amplitude state to the low amplitude state at $y = y_{max}$. Upon re-entering the low amplitude state the transistor is strictly off from $y = y_{max}$ down to $y = y_*$.

pieces are governed by a "slow" set of equations (from the τ parameterization of time). The fast equations,

$$\begin{aligned} \frac{dx}{dt} &= x - x^3/3 - y \\ \frac{dy}{dt} &= 0 \end{aligned} \tag{6}$$

describe the rapid evolution to the slow manifold, $x - x^3/3 - y = f(x, y) = 0$. Once the system has reached the $f(x, y) = 0$ manifold there is a strong ($1/\epsilon$ strong) restoring force on x that keeps the system on the $0 = f(x, y)$ manifold. Because of this the system follows the singular slow equations

$$\begin{aligned} 0 &= x - x^3/3 - y \\ \frac{dy}{d\tau} &= x \end{aligned} \tag{7}$$

along the slow manifold until $\frac{dy}{d\tau} = x$ forces the system off of the slow manifold. At that point the system once again follows Eqs. (6) to find its way to a different piece of the slow manifold.

These two limits for $\epsilon \to 0$, Eqs. (6) and 7, govern the zeroth order SPT solution fragments. The entire zeroth order solution for an entire relaxation cycle is found by linking together the fast and slow pieces. Singular perturbation theory also allows refinements to the zeroth order solution in higher orders of ϵ to be found, at least in principle.

V. SPT APPLIED TO TRANSISTOR EQUATIONS

Ideally we would like to find the fast equations and slow equations for Eqs. (3). This would provide the slow manifold that the system spends most of its time evolving along and would allow us to understand when the system will leave one branch of the slow manifold (the high amplitude state) and move to the other branch of the slow manifold (the low amplitude state), and when it will return to the first branch of the manifold (the high amplitude state). There is, however, a complication. In the case of the van der Pol oscillator the long time solution of the fast equations, Eqs. (6), is a stable fixed point. But the fast equations for Eqs. (3) are

$$\begin{aligned}
\frac{dx_1}{d\phi} &= \gamma[\sin(2\pi\phi) - x_3 - y] \\
\frac{dx_2}{d\phi} &= -\delta[x_1 + 2x_2 - 2\kappa x_3 H(x_3)] \\
\frac{dx_3}{d\phi} &= \delta[x_1 + x_2 - \kappa x_3 H(x_3)] \\
\frac{dy}{d\phi} &= 0
\end{aligned} \tag{8}$$

whose long time limit solution is usually a stable period one limit cycle. (As previously noted, near the transition from the low amplitude state branch of the slow manifold the solution may, for some parameter values, go through a period doubling cascade to chaos. The low frequency switching does not depend on period doubling.)

We therefore would like to find the slow equations for the period one average of Eqs. (3) which would give the slow manifold for the period one limit cycle. However the slow equations for the period one average of Eqs. (3) are

$$\begin{aligned}
0 &= \gamma[- < x_3 > - < y >] \\
0 &= -\delta[< x_1 > +2 < x_2 > -2\kappa < x_3 H(x_3) >] \\
0 &= \delta[< x_1 > + < x_2 > -\kappa < x_3 H(x_3) >] \\
\frac{d < y >}{d\psi} &= \lambda(< x_1 > + < x_2 >) - < y > - y_o
\end{aligned} \tag{9}$$

where $\psi = \epsilon\phi$ and $< z >= \int_{\phi}^{\phi+1} z d\phi/1$ is the average of z over one drive cycle. Solving for the averages gives

$$\begin{aligned}
< x_1 > &= 0 \\
< x_2 > &= \kappa < x_3 H(x_3) > \\
< x_3 > &= - < y > \\
\frac{d < y >}{d\psi} &= \kappa\lambda < x_3 H(x_3) > - < y > - y_o
\end{aligned} \tag{10}$$

which is not a closed set of equations. To find the average $< x_3 H(x_3) >$ one must go back to Eqs. (8) and find the solution to the limit cycle and from that solution calculate the average $< x_3 H(x_3) >$.

Recall that there are not just two, but rather three time scales in this problem. Equations (8) are the fast equations with respect to the switching time parameterization $\psi = \epsilon\phi$, but they are slow with respect to the transistor turn on. To see this first we rescale x_3, which is small in the on state, $X_3 = \kappa x_3$ (recall $\kappa \gg 1$). This gives us the slow parameterization with respect to the turn on time

$$\begin{aligned}
\frac{dx_1}{d\phi} &= \gamma[\sin(2\pi\phi) - X_3/\kappa - y] \\
\frac{dx_2}{d\phi} &= -\delta[x_1 + 2x_2 - 2X_3] \\
\frac{1}{\kappa}\frac{dX_3}{d\phi} &= \delta[x_1 + x_2 - X_3] \\
\frac{dy}{d\phi} &= 0
\end{aligned} \tag{11}$$

If we take the slow limit with respect to the transistor turn on time (i.e., $\kappa \to \infty$) we find

$$\begin{aligned}
\frac{dx_1}{d\phi} &= \gamma[\sin(2\pi\phi) - X_3/\kappa - y] \\
\frac{dx_2}{d\phi} &= -\delta[x_1 + 2x_2 - 2X_3] \\
0 &= \delta[x_1 + x_2 - X_3] \\
\frac{dy}{d\phi} &= 0
\end{aligned} \tag{12}$$

There is also the time parameterization which is fast with respect to the transistor turn on $\xi = \phi\kappa$

$$\begin{aligned}
\frac{dx_1}{d\xi} &= \frac{1}{\kappa}\gamma[\sin(2\pi\phi) - X_3/\kappa - y] \\
\frac{dx_2}{d\xi} &= -\frac{1}{\kappa}\delta[x_1 + 2x_2 - 2X_3] \\
\frac{dX_3}{d\phi} &= \delta[x_1 + x_2 - X_3] \\
\frac{dy}{d\phi} &= 0
\end{aligned} \tag{13}$$

Taking the fast limit ($\kappa \to \infty$) we have

$$\begin{aligned}
\frac{dx_1}{d\xi} &= 0 \\
\frac{dx_2}{d\xi} &= 0 \\
\frac{dX_3}{d\xi} &= \delta[x_1 + x_2 - X_3] \\
\frac{dy}{d\xi} &= 0
\end{aligned} \tag{14}$$

So that in the fast limit, only X_3 evolves and has the solution

$$X_3(\xi) = (x_1 + x_2)(1 - e^{-\delta(\xi - \xi_o)}) \tag{15}$$

where ξ_o is the time at which the transistor turns on (i.e., $X_3(\xi_o) = 0$). And x_3 in terms of ϕ is

$$x_3(\phi) = (\frac{x_1 + x_2}{\kappa})(1 - e^{-\kappa\delta(\phi - \phi_o)}). \tag{16}$$

Since $\kappa\delta \gg 1$ the time required for transistor control variable, x_3, to jump from the value $x_3 = 0$ to $x_3 = \frac{x_1+x_2}{\kappa}$ is exceedingly small and we can reasonably treat the jump in x_3 at the transistor turn on as discontinuous.

The slow limit just described only exists when κ is present in the equations, that is when the transistor is on. When the transistor is off κ falls out of the problem and we must use Eqs. (8). We therefore have two slow branches of Eqs. (8) with respect to the transistor turn on time, namely the On branch for which $H(x_3) = 1$:

$$\begin{aligned} \frac{dx_1}{d\phi} &= \gamma[\sin(2\pi\phi) - (x_1 + x_2)/\kappa - y] \\ \frac{dx_2}{d\phi} &= \delta x_1 \\ x_3 &= (x_1 + x_2)/\kappa \\ \frac{dy}{d\phi} &= 0 \end{aligned} \tag{17}$$

and the Off branch for which $H(x_3) = 0$:

$$\begin{aligned} \frac{dx_1}{d\phi} &= \gamma[\sin(2\pi\phi) - x_3 - y] \\ \frac{dx_2}{d\phi} &= -\delta(x_1 + 2x_2) \\ \frac{dx_3}{d\phi} &= \delta(x_1 + x_2) \\ \frac{dy}{d\phi} &= 0 \end{aligned} \tag{18}$$

The On and Off branches, Eqs. (17) and (18), are linear and can be readily solved. The solution on each branch is composed of a transient piece coming from the autonomous equation and a particular solution which is non-transient. (Recall for a driven harmonic oscillator $\frac{d^2x}{dt^2} - 2\beta\frac{dx}{dt} + x = F(x,t)$ the autonomous solution is the solution to $\frac{d^2x}{dt^2} - 2\beta\frac{dx}{dt} + x = 0$ and has two constants of integration. The particular solution is a solution to $\frac{d^2x}{dt^2} - 2\beta\frac{dx}{dt} + x = F(x,t)$ without any constants of integration. For $\beta \neq 0$ and long times the autonomous solution decays to 0.) Both are important for the long time behavior of the system because of the repetitive switching back and forth between the On and Off branches. The fragments of the period one oscillation from the On and Off branches of the manifold that is slow compared to the transistor turn on time can then be pieced together and solved subject to the following two conditions: that x_1 and x_2 are continuous at each junction (i.e., both the On to Off and Off to On junctions) (as was done for the diode resonator in [7] and [8]) and x_3 is continuous at the junction from Off to On.

Finding period one solutions with one piece each from the On and Off branches is sufficiently complicated as to require a numerical solution. We do this by enforcing the five continuity conditions at two undetermined values of ϕ, ϕ_o and ϕ_1, and then numerically solve for ϕ_o and ϕ_1 such that transistor control variable, $x_3 = 0$, at the transistor turn on and turn off. Within such a scheme finding values for ϕ_o and ϕ_1 is tantamount to finding a potential period one solution. In searching for period one solutions with one piece from the On branch and one from the Off branch, we find a very limited number of solutions. The stable solutions correspond to the period one limit cycles of the large amplitude and low amplitude states. Examples for x_1, x_2, and x_3 in both states with $y = 1.15$ are shown in Fig. 6. The agreement between these waveforms and the numerically integrated waveforms of Fig. 4 is exceptional.

When the low amplitude state or high amplitude state consists of only period one oscillations we can say a bit about the destruction of that state near the switching point. Numerical searches of the solution space for period one oscillations show that for y sufficiently close to the switching point (y_{min} or y_{max} as appropriate) there are two solutions ((a) and (b)) with values of ϕ_o and ϕ_1 ($\phi_o^{(a)}$, $\phi_1^{(a)}$ and $\phi_o^{(b))}$, $\phi_1^{(b)}$ respectively) near each other. As y approaches the switching point the two solutions converge (i.e., $\phi_o^{(a)} - \phi_o^{(b))} \to 0$ and $\phi_1^{(a)} - \phi_1^{(b))} \to 0$). For y closer to the switching point than this convergence our numerical search fails to find a nearby solution.

If the circuit parameters are such that the system passes through a period doubling cascade before switching from the low amplitude state to the high amplitude state, then our period one analysis of the low amplitude state breaks down. The period doubling cascade to chaos is typically entered when the period one solution for the low amplitude state is suddenly destroyed. This state is destroyed when a second local maximum in x_3 pushes up through the transistor turn on value. At this point this formal solution to the period one oscillation is no longer valid because the Off branch solution passes from the Off region into the On region and back into the Off region before it connects with the On region that is assumed to be there.

VI. RANGE AND SWITCHING FREQUENCY

In the previous section we constructed period one orbits for the system using one On and one Off branch of the manifold that is slow with respect to the transistor turn on time. Using the understanding gained will allow us to estimate the frequency of the switching, f_s as a function of frequency f and driving amplitude V_A. First we must search for the values of y at which each of the branches of the slowest manifold, the manifold that determines the low frequency switching, cease to exist. Doing so allows us to determine y_{min} and y_{max} directly from the analysis; y_{min} is the value of y at which the low amplitude branch ceases to exist and y_{max} is the value of y at which the high amplitude branch ceases to exist. We can also determine y_*, in the low amplitude state the transistor remains strictly off over the interval (y_*, y_{max})

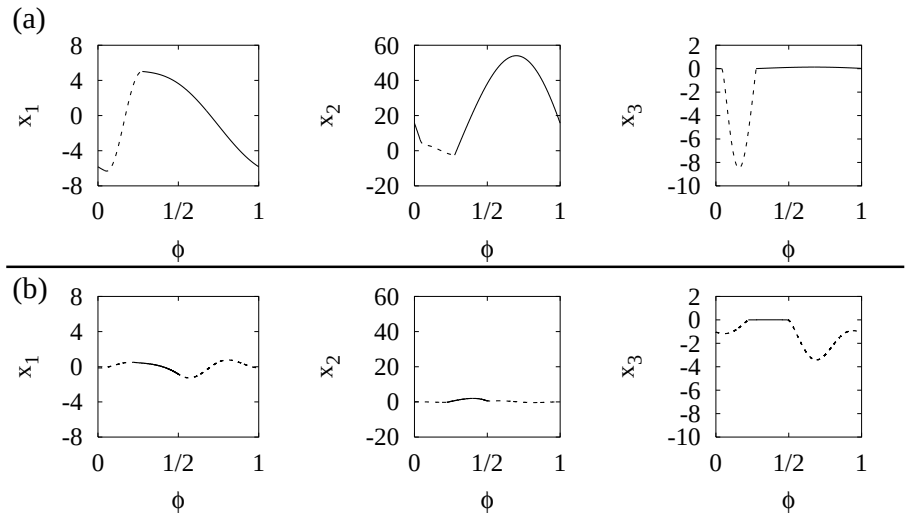

FIG. 6: Solutions for x_1, x_2, and x_3 in the (a) large amplitude state and (b) low amplitude state are found by piecing together an On state (solid line) with an Off state (dashed line) and demanding that the resulting wave form be periodic in the drive frequency. The agreement between these waveforms and the numerically integrated waveforms of Fig. 4 is exceptional.

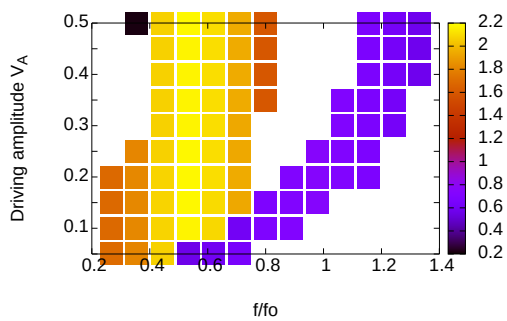

FIG. 7: The range over which y varies, $y_{max} - y_{min}$, as determined from numerical simulations, in the switching system with $fo = 1/\sqrt{4\pi^2 L2C_o}$.

and, as a result, the particular solution (as opposed to the autonomous solution) is the dominant. We therefore define y_* as the largest value of y at which the particular solution of x_3 is tangent to the line $x_3 = 0$. Since the parameters of Eqs. (17) and (18) depend on f but not V_A, the search for y_{min}, y_{max}, and y_* is independent of V_A and need only be done once for each frequency. The results of this search appear in Table 1 and will be discussed shortly.

Figure 7 shows the length of the interval (y_{min}, y_{max}) found by numerical integration of Eqs. (3). Interval length is only displayed for parameter values for which the system switched periodically. There are two distinct bands of switching behavior in this graph: band 1 is present for $f/f_o < 1$ with a large variation in y, and band 2 tends to occur at higher frequency and for which the variation in y is smaller. These two bands arise from qualitatively different behavior. In band 1 the low and high amplitude branches of the slow manifold are both period one, whereas in band 2 the high amplitude branch is period two. This puts a full discussion of band 2 out of the realm of the analysis in this paper.

There are frequencies for which both bands are present for the same frequency but different values of V_A. At these frequencies the high amplitude branch of band 1 is also the low amplitude branch of band 2.

Table 1 lists the range of (y_{min}, y_{max}) from numerical simulation of Eqs. (3) as well as the range found using the above analysis. Although our analysis fails to detect band 2 the agreement between numerical simulations and our analysis is quite good for band 1. Our analysis provides an upper bound for y_{min} and a lower bound for y_{max}, the switch from low amplitude branch to high amplitude branch (and vice versa) will not happen before the low amplitude branch becomes unstable but the system may linger near before switching to the high amplitude branch. In practice the system does not linger long, and we note from Table 1 that as $f/f_o \to 1$ the values of y_{min} and y_{max} from the simulation approach the bound set by our analysis.

In addition to the range over which y varies we need to know how quickly y varies. Recall from Eqs. (10) that it is necessary to compute $\lambda\kappa < x_3 H(x_3) >= \lambda < (x_1 + x_2)H(x_3) >$, which is proportional to the current that flows through the transistor and into the capacitor C while the transistor is on. Instead of computing $\lambda\kappa < x_3 H(x_3) >$ at a dense set of points along the interval (y_{min}, y_{max}), we calculate $\lambda\kappa < x_3 H(x_3) >$ at a few points (y_{min}, $(y_{max} + y_{min})/2$, and y_{max} for the high amplitude state, and only at y_{min} for the low amplitude state because $< x_3 H(x_3) >= 0$ over the interval

TABLE I: A comparison of the range of (y_{min}, y_{max}) from numerical simulation to the range found using the above analysis. Also the value of $\kappa\lambda < x_3 H(x_3) >$ at three values of y where $y_{mid} = \frac{y_{min}+y_{max}}{2}$. For reference y_o ranges from 3 to 30.

Frequency f (kHz)	Simulation (y_{min}, y_{max})	Analysis (y_{min}, y_{max})	$\lambda\kappa < x_3 H(x_3) >$ at $(y_{min}, y_{mid}, y_{max})$
150	$(0.83, 2.52)$	$(0.96, 2.19)$	$(204, 282, 310)$
200	$(0.90, 2.72)$	$(0.98, 2.54)$	$(92.0, 122.6, 145.8)$
250	$(0.83, 2.91)$	$(0.96, 2.80)$	$(48.8, 72.2, 85.2)$
300	$(0.93, 3.11)$ $(0.52, 1.09)$	$(0.93, 3.04)$	$(28.0, 42.4, 49.4)$
350	$(1.23, 3.34)$ $(0.54, 1.14)$	$(1.23, 3.30)$	$(19.7, 26.8, 29.4)$
400	$(1.66, 3.60)$ $(0.55, 1.18)$	$(1.67, 3.58)$	$(13.9, 16.9, 16.4)$
450	$(2.33, 3.93)$ $(0.52, 1.21)$	$(2.34, 3.93)$	$(9.4, 10.2, 9.4)$
500	$(0.51, 1.22)$	$(-)$	$(-)$
550	$(0.48, 1.22)$	$(-)$	$(-)$
600	$(0.51, 1.22)$	$(-)$	$(-)$
650	$(0.53, 1.20)$	$(-)$	$(-)$
700	$(0.54, 1.17)$	$(-)$	$(-)$
750	$(0.54, 1.12)$	$(-)$	$(-)$

$(y_*, y_{max}))$ and linearly interpolate in between.

Our estimates of $\lambda\kappa < x_3 H(x_3) >$, y_{min}, y_{max}, and y_* allow us to integrate the $< y >$ equation of Eqs. (10) (i.e., the one drive cycle average equation for y) over one switching period. We break the integration up into the four regions of Fig. 8. The system evolves around the orbit in Fig. 8 a clockwise sense (i.e., it starts at y_{max} in region 1 and then at y_* passes into region 2, etc.). Integrating the $< y >$ equation of Eqs. (10) and inverting yields the time the system spends in region i:

$$\Delta\phi_i = \frac{1}{\epsilon(\lambda m_i - 1)} \ln\left(\frac{y_{ei} + \tilde{y}_{oi}}{y_{si} + \tilde{y}_{oi}}\right) \tag{19}$$

where $\Delta\phi_i$ is the time spent in region i, y_{si} is the value

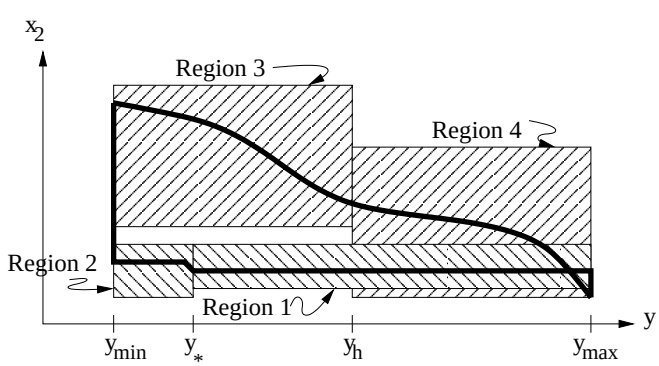

FIG. 8: The four regions over which the integration has been broken to find the switching frequency, f_s. The system goes around the orbit in a clockwise rotation.

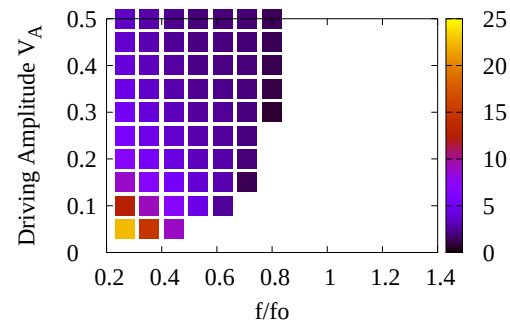

FIG. 9: The normalized switching frequency, $F_s = \tau_{RC} f_s = R_e C f_s$, as determined from the above analysis. The switching system has a natural frequency $fo = 1/\sqrt{4\pi^2 L 2C_o}$. Only band 1 appears because our analysis does not apply to band 2.

of y at the start of the region, y_{ei} is the value of y at the end of the region, $\tilde{y}_{oi} = \frac{\lambda b_i - y_o}{\lambda m_i - 1}$, and the linearization of $\lambda\kappa < x_3 H(x_3) >$ has parameters m_i and b_i such that $m_i y + b_i \approx \lambda\kappa < x_3 H(x_3) >$ in region i. For example, in region 1 $y_{s1} = y_{max}$, $y_{e1} = y_*$, $m_1 = b_1 = 0$, and $\tilde{y}_{o1} = -y_o$. Summing the time contribution from all four regions yields our estimate of the slow switching period T_s and the switching frequency $f_s = 1/T_s$. In Fig. 9 we present the normalized switching frequency, $F_s = \tau_{RC} f_s$ where $\tau_{RC} = R_e C$, for a range of fs and V_As.

Notice that for a fixed value of f, some values of V_A have an estimate for F_s and others there is none. For those that do not, either the value of $\kappa\lambda < x_3 H(x_3) >$ at y_{min} on the high amplitude branch was so small that $< y >$ would not grow (i.e., $\kappa\lambda < x_3 H(x_3) > |_{\text{at } y=y_{min}} - y_{min} - y_o < 0$), or the high amplitude branch became stable (i.e., $\kappa\lambda < x_3 H(x_3) > |_{\text{at } y=y_{min}} - y_{min} - y_o > 0$ but either $\kappa\lambda < x_3 H(x_3) > |_{\text{at } y=y_h} - y_h - y_o < 0$ or $\kappa\lambda < x_3 H(x_3) > |_{\text{at } y=y_{max}} - y_{max} - y_o < 0$). Each of these estimates is for a band 1 f_s. Band 2 oscillations are possible in regions where band 1 oscillations are not because the period two high amplitude branch in band 2 has a large enough DC bias to charge C, even at lower values of V_A when the period one high amplitude branch cannot.

We now wish to compare our results to those of numerical integration of the whole system. Towards this end we must calculate the switching frequency, f_s, from the numerical integration of Eqs. (1). From the time series we find the times of each maxima in the variable y and record the average interval between maxima, $< T_{int} >$, when the standard deviation in the intervals is less than $< T_{int} > /4$. This is to exclude parameter values for which the behavior is non-periodic in na-

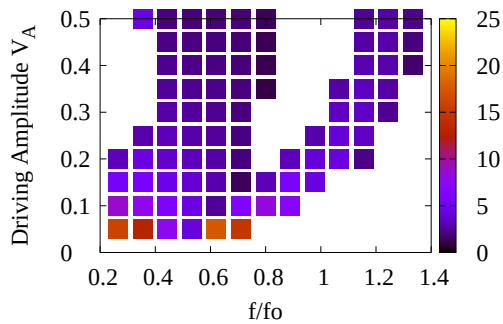

FIG. 10: The normalized switching frequency, F_s, as deduced from numerical simulations by the technique described in the text. The switching system has a natural frequency $fo = 1/\sqrt{4\pi^2 L2C_o}$.

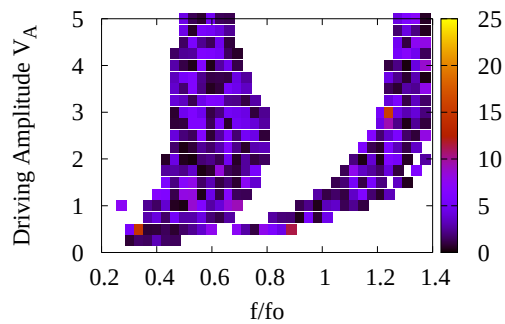

FIG. 11: The normalized switching frequency, F_s, from the experiment in [1] where $f_o \approx 693kHz$.

ture. This excludes some data for low frequencies and larger driving amplitudes ($f/f_o \leq 0.4$, $V_A > 0.25$) that is closer to bursting in behavior. The record of this for a range of fs around the natural frequency of the system, $f_o = 1/\sqrt{4\pi^2 L2C_o}$, and a range of driving amplitudes V_As appears in Fig. 10. (The natural frequency depends on $2C_o$ instead of C_o because the internal capacitors are parallel, and so their capacitances add.)

Within band 1 the agreement is quite good for higher driving frequencies. At lower driving frequencies the analysis suggests that there is switching behavior where the numerical simulation does not. If one consults Table 1, one can see that as f decreases the $\lambda\kappa < x_3 H(x_3) >$ becomes large. The SPT analysis is predicated on assumption that $\frac{d<y>}{d\phi}$ is much less than $\frac{dx_j}{d\phi}$ where $j = 1$, 2, and 3, which may not be the case if $\lambda\kappa < x_3 H(x_3) >$ is becoming large.

By considering the normalized switching frequency, F_s, instead of f_s we are able to compare our analysis and numerical integration with the results of the experimental work in [1] which are reproduced in Fig. 11. We chose a smaller value of τ_{RC} (recall that $\tau_{RC} = R_e C$) for the numerical integration so that the integration could be done in a reasonable amount of time. For the experimental circuit $\tau_{RC} \approx 1.24$, for the numerical work the $\tau_{RC} = 0.03$, and for the analytical work no assumption was necessary (from Eq. (19) f_s is proportional to $\epsilon = \frac{1}{fR_eC}$ and F_s is proportional to $\epsilon\tau_{RC} = 1/f$).

There are several aspects of the experimental results from the circuit in Fig. 1 that are accounted for in the numerical integration and analysis of the simpler circuit in Fig. 3. The experimental results in Fig. 11 show two bands, one on either side of $f/f_o = 1$. This is the same basic structure found in the numerical simulation. With regard to the analysis we note that band 1 of the analysis extends over to and no further than $f/f_o = 0.8$, as is also the case for band 1 of the experimental results in Fig. 11. With regard to the switching frequencies, note that the majority of the values for F_s from our analysis and numerical integration fall within the same range of values as those found in the experiment.

VII. CONCLUSION

We have shown that the low frequency switching in a class C amplifier, due to a modest amplitude signal at a frequency higher than the circuit was designed to operate at, can be understood using a singular perturbation analysis. In particular, by analyzing the high frequency (input signal frequency) response of the system we have been able to estimate the frequency of the slow behavior of the system. We also are able to predict one band of driving frequencies and amplitudes over which the slow behavior occurs. We expect that the techniques described in this paper could be extended to find the second observed band of driving frequencies and amplitudes over which the slow behavior occurs.

REFERENCES

[1] T.L. Carroll, Phys. Rev. E **67**, 046208 (2003). 2-10
[2] T.L. Carroll and L.M. Pecora, Phys. Rev. E **66**, 046219 (2002).
[3] E.R. Hunt and R.W. Rollins, Phys. Rev. A **29**, 1000 (1984).
[4] C.H. Kim, C.H. Cho, C.S. Lee, J.H. Yim, J. Kim, and Y. Kim, Phys. Rev. A **38**, 1645 (1988).
[5] P.S. Linsay, Phys. Rev. Lett. **47**, 1349 (1981).

[6] Z. Su, R.W. Rollins, and E.R. Hunt, Phys. Rev. A **40**, 2698 (1989).
[7] N. Takeuchi, T. Nagai, and T. Matsumoto, Electron. Commun. Jpn. **84**, 91 (2001).
[8] S. Tanaka, S. Higuchi, and T. Matsumoto, Phys. Rev. E **54**, 6014 (1996).
[9] J. Testa, J. Perez, and C. Jeffries, Phys. Rev. Lett. **48**, 714 (1982).
[10] R.M.D. de Morales and S. Anlage, Phys. Rev E **68**, 26201 (2003).
[11] An excellent discussion of SPT in general and the subtleties of the van der Pol oscillator can be found in: R.E. O'Malley, *Singular Perturbation Methods for Ordinary Differential Equations*, (Springer-Verlag, New York, 1991).